

Measuring colloidal interactions with confocal microscopy

C. Patrick Royall

Institute of Industrial Science, University of Tokyo, 4-6-1 Komaba, Meguro-ku, Tokyo 153-8505, Japan and School of Chemistry, University of Bristol, Bristol, BS8 1TS, United Kingdom

Ard A. Louis

Department of Physics, University of Oxford, Oxford OX1 2JD, United Kingdom

Hajime Tanaka

Institute of Industrial Science, University of Tokyo, 4-6-1 Komaba, Meguro-ku, Tokyo 153-8505, Japan

(Received 2 May 2007; accepted 13 June 2007; published online 30 July 2007)

We use confocal laser scanning microscopy to measure interactions in colloidal suspensions. By inverting the radial distribution function, determined by tracking the particle coordinates, we obtain the effective interaction between the colloidal particles. Although this method can be applied to arbitrary colloidal interactions, here we demonstrate its efficacy with two well-known systems for which accurate theories are available: a colloid-polymer mixture and binary hard spheres. The high sensitivity of this method allows for the precise determination of complex interactions, as exemplified, for example, by the accurate resolution of the oscillatory effective potential of the binary hard sphere system. We argue that the method is particularly well suited for the determination of attractive forces. © 2007 American Institute of Physics. [DOI: 10.1063/1.2755962]

I. INTRODUCTION

Colloidal dispersions find ever-increasing industrial and household applications, and underpin many biological processes. Their behavior is driven by the interactions between the various components: colloidal particles, solvent molecules, and other species, such as ions and (macro-) molecules. The complexity of these systems, and the spatial and dynamic asymmetry between the colloidal particles (10 nm–1 μm) and smaller molecular and ionic species, has led to the development of coarse-graining schemes where the smaller components are formally integrated out.¹ This generates a one-component picture, where only the *effective* colloid-colloid interactions need to be considered, and the complexity of the description is vastly reduced. The colloid behavior in the original complex system may then be faithfully reproduced by appeal to liquid state theory² and computer simulation.³ Since colloidal dispersions are easy to manipulate and observe, and exhibit liquid and crystal phases reminiscent of atomic and molecular systems, along with nonergodic states such as glasses and gels, a range of fundamental questions of condensed matter science may be tackled.^{4–6} Understanding colloidal behavior furthers the development of advanced materials, such as photonic crystals,⁷ and provides insight into industrially and biologically relevant problems, including jamming,⁸ protein crystallization,⁹ and condensation diseases such as eye cataracts and Alzheimer's.¹⁰

Central to this one-component approach is the use of a suitable colloid-colloid interaction $u(r)$. Notable early successes include the Derjaguin, Landau, Verwey, and Overbeek theory of charged colloids¹¹ and the Asakura-Oosawa (AO) theory of colloids in a solution of macromolecules,¹² subsequently popularized by Vrij.¹³ While theories such as these have been used to describe colloidal model systems in which

the interactions may be tailored with very considerable success,^{4,6,14} the general situation is often considerably more complex.

One is therefore faced with the question of how to measure an arbitrary effective colloid-colloid interaction. There has been much recent progress using single particle techniques. The interaction between a colloid and a glass wall can be accurately measured with total internal reflection microscopy,^{15,16} while the interaction between two colloids confined to a line can be measured by optical tweezers.^{17–19} One attraction of these methods is that no *a priori* assumption need be made about the effective colloid-colloid interaction, allowing for a robust test of theory. However, the use of these methods is not always straightforward. For example, in the case of optical tweezers, relatively small and subtle experimental errors were shown to lead to the wrong *sign* of the interaction of charged colloids.^{20,21} Another limitation of these methods is that it is difficult (although in principle possible²²) to measure colloid interactions at finite concentrations.

An alternative approach is to measure correlation functions and invert them to extract the effective potentials. Traditionally this has been achieved by scattering techniques that measure the reciprocal space structure function $S(k)$.^{2,23,24} However, a fundamental difficulty with these techniques arises because the inversion of $S(k)$ is a poorly conditioned problem. Many different forms of repulsive interactions can all be surprisingly well fitted to the $S(k)$ of a hard sphere fluid.² Similarly, multiple different strong attractive interactions generate an $S(k)$ that is close to the form given by the Baxter sticky hard sphere model,^{25,26} suggesting that not much more is being measured than the second virial coefficient.

More recently, the advent of real-space techniques such

as confocal microscopy has allowed the direct determination of the colloidal radial distribution function $g(r)$,^{27,28} and very recently used to make high-precision measurements of binary colloids in two dimensional (2D).²⁹ Just as in the case for $S(k)$, the radial distribution function can also be inverted to extract an effective potential $u(r)$.^{28,30} At higher densities, there are subtleties involved in extracting potentials from pair structure, especially when many-body effects are present.³¹ These have been measured quantitatively in the case of charged colloids^{30,32} and colloids interacting via a magnetic dipole.³³ However, in the low density limit the interpretation is straightforward:

$$\lim_{\rho \rightarrow 0} g(r) = \exp(-\beta u(r)), \quad (1)$$

where $\beta=1/k_B T$, k_B is Boltzmann's constant, and T is the absolute temperature. This limit also suggests that extracting potentials from an experimentally determined $g(r)$ is a better conditioned problem than its reciprocal space counterpart. In particular, attractive components of the potential will be magnified exponentially. At finite densities the $g(r)$ depends in a more complex manner on $u(r)$, but there exist integral equation and Monte Carlo inversion techniques that can be used for inversions.³⁴ Moreover, it has been argued^{26,35} that for strongly attractive potentials, Eq. (1) remains a remarkably accurate approximation even at finite (but still modest) colloid concentrations.

In this paper we propose that measuring the radial distribution function $g(r)$ by confocal microscopy provides a reliable route to the effective pair interaction, particularly for the attractive components of the potential. Our method makes no *a priori* assumption about the nature of the effective pair interaction, and so it may be applied to systems of arbitrary complexity, without recourse to theory. We measure the radial distribution function $g(r)$ directly in three dimensional (3D) with confocal microscopy,²⁸ avoiding any possible artifacts from Fourier transforming reciprocal space data, or perturbation of the system by introducing an optical tweezers to the suspension. To test our method, we consider systems for which the interaction is well understood from theory: a colloid-polymer mixture¹² and binary colloidal "hard spheres."³⁶ In the case of the binary hard sphere fluid, in addition we find the first *quantitative* agreement with theory for the effective interaction between the large particles along with the first 3D resolution of the correlation functions for the smaller particles.

A schematic of the systems we consider is shown in Fig. 1, along with the effective interactions between the large colloids used for the binary hard sphere system.³⁶ This paper is organized as follows: in Sec. II we describe our experimental and analysis methodology. Section III identifies key model interactions and outlines the Monte Carlo simulation employed. After direct visualization of the systems under investigation with confocal microscopy images, Sec. IV compares theoretical, simulated, and experimental radial distribution functions. This is followed by direct application of Eq. (1) to yield the effective colloid-colloid interaction. We

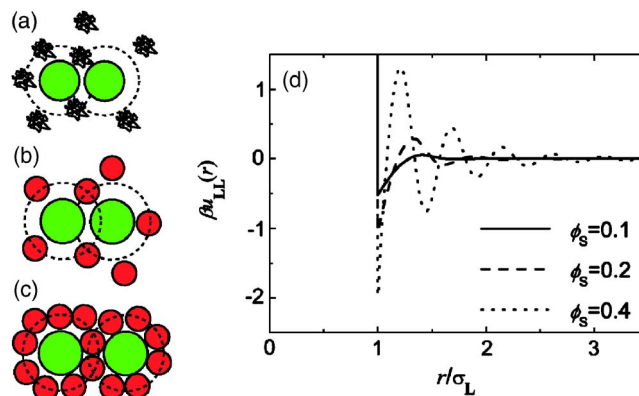


FIG. 1. (Color online). Schematics of the systems considered. (a) Colloid-polymer mixture. The dashed lines show depletion zones, into which polymer centers of mass may not enter. When two colloids approach such that these zones overlap, the polymer entropy increases, which leads to an effective attraction between the colloids (Ref. 12). (b) Depletion zones around two colloids in a dilute solution of smaller colloids. (c) Depletion zones around two colloids in a concentrated solution of smaller colloids. The correlations between the smaller colloids can lead to an oscillatory pair potential, shown in (d) where effective large colloid pair potentials, calculated from density functional theory (Ref. 36), are depicted as a function of small colloid volume fraction ϕ_s .

also consider large-small and small-small correlations in binary hard spheres and conclude with a discussion and outlook in Sec. V.

II. EXPERIMENTAL SYSTEM

We used polymethylmethacrylate colloids, sterically stabilized with polyhydroxyl steric acid. The colloids were labeled with 4-chloro-7-nitrobenzo-2-oxa-1,3-diazol (NBD) and rhodamine isothiocyanate in the case of the large and small colloids, respectively.³⁷ The use of two different dyes enabled us to distinguish both species. The polydispersity was determined with static light scattering to be 3% for the large ($\sigma=2.4 \mu\text{m}$) and 5% for the small ($\sigma=1.2 \mu\text{m}$) colloids. In the binary hard sphere system, the small-large colloid size ratio $q=0.5$.

The polymer used was polystyrene, with a molecular weight of 3.1×10^7 , here $M_w/M_n=1.3$. We estimate the polymer radius of gyration as $R_G=160 \text{ nm}$ in an ideal solvent.³⁸ Here the solvent may be regarded as "good," since the experiments were conducted at room temperature, some 80°C above the theta temperature for this solvent mixture, as deduced from phase separation studies of the polymer solution. Some swelling of the polymer coils may therefore be expected. We estimate the swelling as to be 25%–40%,³⁹ and within these bounds treat it as a fit parameter in our description of the colloid-colloid interactions (Sec. III), arriving at a value of 35%, or $R_G \approx 200 \text{ nm}$, leading to a polymer-colloid size ratio $q=0.18$.

To match as much as possible both the colloid density and refractive index, we used a solvent mixture of *cis*-decalin and cyclohexyl bromide. Due to the steric stabilization and refractive index matching, the van der Waals interactions are reduced to a fraction of the thermal energy and can therefore be neglected. We note that sterically stabilized colloids in nonaqueous solvents allow us to probe the interactions al-

most all the way to contact. This is in contrast to aqueous systems often used, where the charge stabilization necessary to prevent aggregation can somewhat hamper measurements close to contact.^{18,19} To screen any (weak) electrostatic interactions, we dissolved tetrabutyl ammonium bromide salt to a concentration of 300 nM in the case of the binary hard spheres⁴⁰ and to 4 mM concentration in the case of the colloid-polymer mixture.⁴¹ The estimated Debye screening lengths are 100 and 13 nm, respectively, well below the characteristic depletion interaction ranges of both systems.

We fix the (large) colloid volume fraction at $\phi_C = \frac{1}{6}\pi\sigma^3\rho = 0.050 \pm 0.005$, where ρ is the number density and σ the diameter. The data were collected on a Leica SP5 confocal microscope, using 488 and 532 nm laser excitations for the NBD and rhodamine labeled colloids, respectively. The microscope was fitted with a resonant scanner and operated at a typical scan rate of 20xy frames per second. Typically 128 frames were taken per 3D image. Combining these op-

tical sections into 3D images allowed us to track the coordinates of each particle as previously described with a precision of around 100 nm.²⁸ Each $g(r)$ was sampled from 8–12 independent 3D images, containing 20–30 000 particles in total. All images were recorded at least 20 μm from the edge of the sample, and we found no evidence of wall-induced layering. We note that it is possible to consider xy data only, we have found that in the case of a 3D system this entirely fails to reproduce the pair structure, due to contributions from out-of-plane particles which are not excluded, due to the limited axial resolution. We therefore work exclusively in 3D.

III. SIMULATIONS AND MODEL INTERACTIONS

The seminal theory of colloid-polymer mixtures is that of Asakura and Oosawa.¹² This AO model leads to a pair interaction between two hard colloidal spheres in a solution of ideal polymers which reads

$$\beta u_{\text{AO}}(r) = \begin{cases} \infty & \text{for } r < \sigma \\ \frac{\pi(2R_G)^3 z_{\text{PR}} (1+q)^3}{6 q^3} \left\{ 1 - \frac{3r}{2(1+q)\sigma} + \frac{r^3}{2(1+q)^3 \sigma^3} \right\} & \text{for } r \geq \sigma < \sigma + (2R_G) \\ 0 & \text{for } r \geq \sigma + (2R_G), \end{cases} \quad (2)$$

where the polymer fugacity z_{PR} is equal to the number density ρ_{PR} of ideal polymers in a reservoir at the same chemical potential as the colloid-polymer mixture. Thus within the AO model the effective temperature is inversely proportional to the polymer reservoir concentration. The polymer-colloid size ratio $q = 2R_G/\sigma$, where R_G is taken as the polymer radius of gyration, and σ is the colloid diameter. Although more accurate potential forms can be derived for interacting polymers,⁴² here we nevertheless use the simpler AO form (2) since for this small size ratio and the relatively low polymer reservoir volume fraction $\phi_P = \frac{4}{3}\rho_{\text{PR}}R_G^3$ used, the differences are expected to be on the order of just a few percent.⁴²

For the binary hard sphere system, we used a potential $\beta u_{\text{BHS}}(r)$ taken from an analytical parametrization of the density functional theory (DFT) results of Roth *et al.*,³⁶ plotted in Fig. 1, which are known to closely match computer simulations. For both the colloid-polymer mixture and the binary hard spheres, the mapping between the depletant reservoir and the experimental system is obtained from Widom's particle insertion method.⁴³

In the colloid-polymer mixture, the effects of charge were found to be negligible. For the binary hard sphere suspension, the electrostatic interactions are weak and screened such that the repulsion amounted to only around $1k_B T$ at contact and the Debye length of around 100 nm (Ref. 44) was much shorter than the depletion interaction induced by the small colloids (1.2 μm). Nevertheless some residual effect of charge was observed when the $g(r)$ obtained from

Eq. (1) was compared with the experimental results. In particular, the first peak was somewhat lower, suggesting that the attractive well at contact was somewhat shallower than anticipated. Therefore, in order to model the interactions more accurately, in addition to the effective interaction $u_{\text{BHS}}(r)$,³⁶ we used the screened Coulomb interaction (neglecting van der Waals interactions due to the refractive index matching).¹¹ This was included by adding a Yukawa (screened Coulomb) potential to the binary hard sphere effective interaction:

$$\beta u_{\text{YUK}}(r) = \begin{cases} \infty & \text{for } r < \sigma \\ \beta\epsilon \frac{\exp(-\kappa(r-\sigma))}{r/\sigma} & \text{for } r \geq \sigma, \end{cases} \quad (3)$$

where r is the center to center separation of the two colloids. The contact potential is given by

$$\beta\epsilon = \frac{Z^2}{(1 + \kappa\sigma/2)^2} \frac{l_B}{\sigma}, \quad (4)$$

where Z is the colloid charge, κ is the inverse Debye screening length, and l_B is the Bjerrum length. In order to estimate the colloid charge, we fitted the height of the first peak of the radial distribution function by varying the potential at contact, determining a value of $(200 \pm 50)e$ for the colloid charge ($\beta\epsilon = (1 \pm 0.5)k_B T$). This value is consistent with the previous work on this system,⁴⁴ and we found similar agreement at all state points considered, and we therefore fix $\beta\epsilon = 1k_B T$ throughout the treatment of the binary hard spheres. We

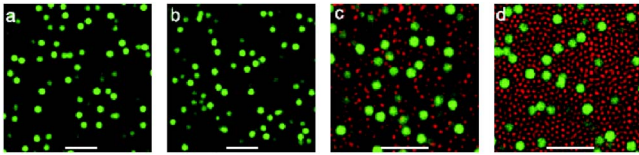


FIG. 2. (Color online). Confocal microscopy snapshots of the systems investigated. (a) “Hard sphere” colloidal fluid, $\phi_c=0.05$. (b) Colloid-polymer mixture, $\phi_c=0.05$, $c_p=3.58 \times 10^{-4}$. Polymers not shown. (c) Binary hard sphere colloidal suspension, $\phi_L=0.05$, $\phi_S=0.10$. (d) Binary hard sphere colloidal suspension, $\phi_L=0.05$, $\phi_S=0.40$, dynamically arrested state. Bars = 10 μm .

stress that although the Yukawa repulsion is not determined with high accuracy, it is only included as a perturbation. A more accurate determination of the colloid charge in these nonaqueous systems would be challenging indeed, especially at moderate or high colloid volume fraction, but our radial distribution function analysis has been tested successfully against electrophoretic measurements at low colloid concentrations.⁴⁵ We therefore believe this to be suitable treatment of a relatively small, yet observable, deviation from hard sphere behavior.

It is important to take into account the polydispersity of the colloids, and the fact that the coordinate tracking generates an intrinsic error. To reproduce the experimental radial distribution functions, we therefore performed Monte Carlo (MC) simulations in the canonical ensemble.³ The 3% polydispersity is directly included as a Gaussian distribution of colloid diameters. Coordinate tracking errors are incorporated by adding a Gaussian noise term of standard deviation 100 nm to coordinates when calculating $g(r)$. The effective colloid-colloid interactions used in the simulations are taken from Eq. (2) for the colloid-polymer mixture and from the DFT potentials of Roth *et al.*,³⁶ together with Eq. (3), for the binary hard sphere case.

IV. RESULTS

A. Colloid-polymer mixture radial distribution functions

Real-space confocal microscopy images of the systems studied are illustrated in Fig. 2. A hard-sphere-like dispersion is shown in Fig. 2(a). As might be expected for relatively dilute hard spheres, little structure is evident. Figure 2(b) is a colloid-polymer mixture with a polymer weight fraction c_p of 3.58×10^{-4} . Note the increased number of closely approaching colloids in the case of added polymer, providing direct visual evidence of attractions.

The connection between interactions and structure in the colloid-polymer mixture is more quantitatively demonstrated in Fig. 3, which depicts radial distribution functions $g(r)$ at varying polymer concentrations. The experimental data directly reveal a rise in the peak of $g(r)$ with increasing polymer concentration, as expected for a depletion interaction. To make a more quantitative comparison we also plot $g(r) \approx \exp(-\beta u_{AO}(r))$, which closely resembles the real $g(r)$ for a perfect AO system at these densities,³⁵ as well as the MC simulations which take into account the polydispersity and the intrinsic coordinate tracking errors. The MC results show

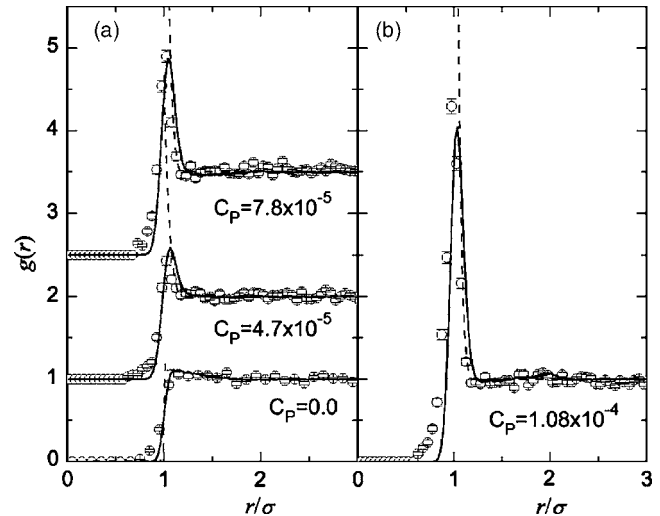


FIG. 3. Radial distribution functions $g(r)$ of colloid-polymer mixtures at various polymer concentrations. Monte Carlo simulations with polymer reservoir volume fraction ϕ_{PR} , according to Eq. (2) (solid lines), are compared to the experimental results (circles). Dashed lines correspond to the relation $g(r) \approx \exp(-\beta u_{AO}(r))$. Monte Carlo simulations consider experimental resolution and polydispersity. (a) Low polymer concentration $C_p < 0.001$. (b) High polymer concentration $C_p > 0.001$.

how the first attractive peak is broadened due to the combined effects of polydispersity and particle tracking accuracy. The near quantitative agreement between the MC simulations and the experiment suggests that this system is well described by the AO depletion potential.¹² In other words, even when the experimental resolution makes a significant impact on the measurement, we may nevertheless access the effective pair potential for different polymer concentrations, using confocal microscopy and MC simulation. There is a tendency for the experimental results to peak slightly to the left of the MC results in Fig. 3. This effect is possibly due to a non-Gaussian error in particle tracking, in the case of closely approaching particles, as noted in the case of 2D particle tracking.²⁰

B. Binary hard sphere radial distribution functions

Confocal microscopy images of the binary hard sphere system investigated are shown in Figs. 2(c) and 2(d). The image with a low density of small colloids ($\phi_S=0.1$), Fig. 2(c), reveals the possibility of imaging both species. At higher concentrations ($\phi_S=0.4$), Fig. 2(d), the images clearly show a pronounced layering of the small particles around the large ones. These correlations are expected to affect both the effective colloid-colloid interactions and the concomitant correlation functions.

The radial distribution functions for the large colloids are depicted in Fig. 4 for increasing concentration of the small colloids. To test Eq. (1), we again compare the experimental results to theory. Overlaying the experimental radial distribution function with $g(r) = \exp[-\beta(u_{BHS}(r) + u_{YUK}(r))]$ (Fig. 4, dashed lines) we see a near quantitative agreement, especially for the higher-order correlations. Using the same potentials, we also carried out MC simulations to include the particle tracking errors and colloid polydispersity. The results are shown in Fig. 4 (solid lines). Although the radial distri-

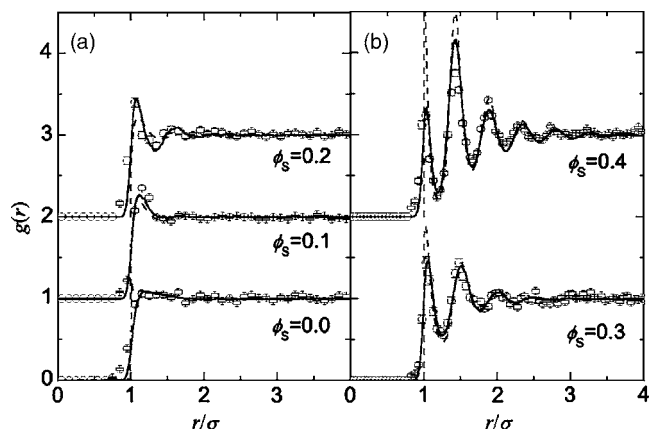


FIG. 4. Radial distribution functions $g(r)$ of large colloids in binary “hard spheres” at various concentrations of the smaller species. MC simulations with small colloid volume fraction ϕ_s (Ref. 36) (solid lines) are compared to the experimental data (circles) as black lines. Dashed lines correspond to the relation $g(r) \approx \exp[-\beta(u_{\text{BHS}}(r) + u_{\text{YUK}}(r))]$. In addition to experimental resolution and polydispersity, MC simulations account for residual colloid charge. (a) Low small colloid concentration, $\phi_s < 0.25$. (b) High small colloid concentration, $\phi_s > 0.25$.

bution functions are less sensitive to the inclusion of polydispersity and tracking errors than in the colloid-polymer mixture case, there is nonetheless an improved agreement with the experimental data, especially close to contact. The good agreement between experiment and theory suggests that, in this case, many-body contributions, which we have not considered, are relatively small.

The interplay between AO-like depletion at low ϕ_s (non-interacting small particles) and the emergence of small-small correlations at higher ϕ_s is well captured in the radial distribution functions. At low ϕ_s , correlations are small and the $g(r)$ resemble those of a colloid-polymer mixture at similar parameters. By contrast, at high ϕ_s , the small particle correlations induce long-ranged oscillations in $g(r)$ and, by extension, also in the effective interaction $\beta u_{\text{BHS}}(r)$.

The binary hard sphere suspension with a small colloid volume fraction of $\phi_s = 0.4$ was, in fact, a nonequilibrium dynamically arrested state. In other words, confocal microscopy revealed no motion, either of the larger or the smaller particles, on a time scale of minutes. In the dilute limit, the characteristic time to diffuse one radius is 29 s for the large particles. The assumptions of Eq. (1) are only valid in dilute ergodic fluids, which clearly does not include dynamically arrested states. Bearing this in mind, we nonetheless compare the radial distribution functions determined experimentally with MC simulation and the equilibrium density functional theory³⁶ used in Eq. (1) with both $g = \exp[-\beta(u_{\text{BHS}}(r) + u_{\text{YUK}}(r))]$ and MC simulation. Perhaps surprisingly, the agreement seems reasonable, considering that the simulation was ergodic, consistent with the relatively weak interactions, Fig. 4(b). However, the small discrepancies in the radial distribution functions, particularly in the height of the second peak, may be related to the nonequilibrium nature of the experiment. We note that the combined volume fraction here is $\phi_L + \phi_s = 0.45$, and even the weak, screened, electrostatic repulsion may be sufficient to promote crystallization at this colloid volume fraction in the case of a

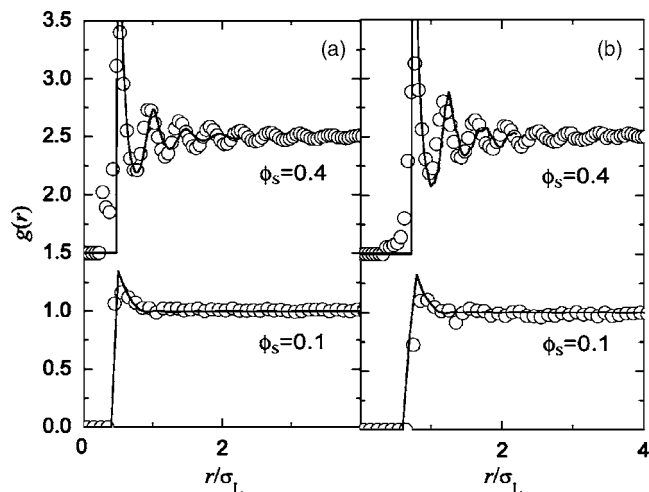


FIG. 5. Cross correlation functions of binary hard spheres. (a) Small-small correlations $g_{\text{SS}}(r)$ at the small colloid volume fractions ϕ_s shown. (b) Large-small correlations $g_{\text{LS}}(r)$ at the ϕ_s shown. The sharper peaks at contact in the simulation data may be attributed to the fact that we considered monodisperse hard spheres and ignored any experimental particle tracking inaccuracies in the MC simulation.

single colloid species.⁴⁴ Crystallization is suppressed here by the inclusion of the larger colloids, leading to the dynamically arrested state observed. It is possible that the discrepancy between the ergodic simulations and nonergodic experiments may be related to these weak electrostatic interactions, in particular, between the majority small colloids, which are not considered in $u_{\text{BHS}}(r)$.

We also succeeded in tracking the coordinates of the small colloids. This enabled us to move beyond the “one-component” picture and treat the large and small particles on an equal footing. Two such cross and small-small correlation functions, $g_{\text{LS}}(r)$ and $g_{\text{SS}}(r)$, are shown in Fig. 5. We note, in particular, the long-ranged correlations in the dynamically arrested state, $\phi_s = 0.4$. In this case we carried out MC simulations in the full binary hard sphere mixture and compared again with the experimental results. Here the simulations only consider monodisperse hard spheres. Despite the tracking errors which are relatively more significant for the small colloids, we nevertheless obtain reasonable agreement between experiment and simulation.

C. Measuring the interactions

1. Binary hard sphere mixtures

We argued in the Introduction that the advantage of measuring $g(r)$ was that, in particular, for systems dominated by strong attractive potentials, the inversion to an effective potential $u(r)$ was better conditioned than the more common reciprocal space techniques. Figure 6 shows direct comparisons of the effective pair potential for the binary hard sphere (HS) system, obtained by invoking the simplified inversion [Eq. (1)] which is expected to be accurate for these parameters. In Fig. 6(a) there are no small spheres, and this benchmark HS potential is well captured with our method. The development of the effective potential between the large colloids with increasing concentration of the small colloids is shown in Figs. 6(b)–6(e). The gradual increase in interac-

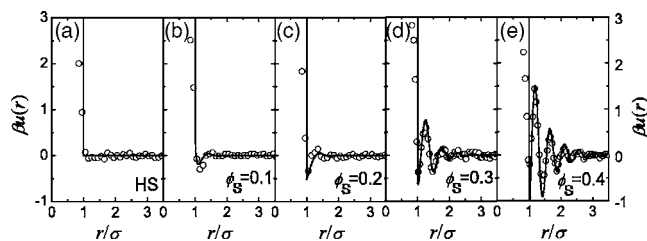


FIG. 6. Effective pair potentials $u(r)$ obtained directly from pair correlation functions. Circles denote experimental data, obtained from the measured $g(r)$ through Eq. (1). (a) Pure “hard spheres.” (b)–(e) Binary hard sphere potentials are calculated with DFT (Ref. 36). These potentials are also depicted in Fig. 1.

tions from weak depletion, with very few correlations (AO like) at low small colloid density [Fig. 6(b)], to a highly developed oscillatory potential is demonstrated. Note that the small spheres generate a much longer-ranged correlation between the large spheres than the polymers [Figs. 6(d) and 6(e)]. The agreement with theory, as extracted by Eq. (1) using $u(r) = u_{\text{BHS}}(r) + u_{\text{YUK}}(r)$, is particularly good, especially at larger distances. We note that these interactions were extracted from experiments without the need for any fit parameters. In particular, the oscillatory portion of the potentials is resolved in near quantitative agreement with theory. This contrast with pioneering results obtained with optical tweezers,¹⁹ which although they demonstrated oscillations, could not be quantitatively fitted to DFT results, even when polydispersity and related effects were taken into account.⁴⁶

2. Colloid-polymer mixtures

Whereas the radial distribution functions for the binary HS mixture could be inverted accurately without the need to explicitly include the effects of polydispersity and tracking errors, the case is not quite so clear-cut for the colloid-polymer mixtures. We show in Fig. 7 the potential for $c_P = 0.288$ mg/l, extracted via Eq. (2). The agreement is clearly not as good as for the binary HS case. The primary reason is that the potential range is considerably smaller, and so coor-

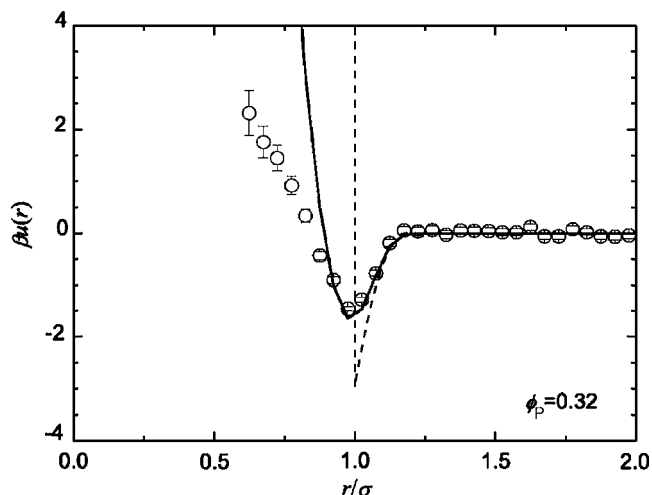


FIG. 7. Effective pair potential $u(r)$ for a colloid-polymer mixture at $\phi_p = 0.32$ obtained directly from the measured pair correlation functions through Eq. (1) and compared to AO theory (dashed line) and to a potential with additional noise convolved through (solid line).

minate tracking errors and polydispersity contributions are more pronounced. It is tempting to regard this as a convolution operation

$$u_{\text{EXP}}(r) = p(r) \oplus u(r), \quad (5)$$

where $u_{\text{EXP}}(r)$ is the measured effective pair potential (for example, that shown in Fig. 7) and $p(r)$ is a blurring function. Deconvolution⁴⁷ with a suitable choice of $p(r)$ may recover a good estimate for the true effective pair potential $u(r)$. However, the discontinuous nature of $u_{\text{AO}}(r)$ [Eq. (2)], due to the hard core, somewhat complicates the convolution operation. Therefore, we convolve the radial distribution function obtained from Eq. (1) instead, and use the same equation to obtain a “blurred” $u(r)$. The agreement with the experimental data is much better than the original potential, suggesting that deconvolution may well yield potentials with higher resolution than can be obtained by direct application of Eq. (1). Here we set $p(r)$ as a Gaussian of standard deviation 120 nm, a value comparable to the tracking error and colloid polydispersity. More sophisticated treatments might deal with the non-Gaussian particle tracking errors, which may result in improved agreement for small r .

V. CONCLUSIONS

In short we have demonstrated a method to directly and quantitatively access effective interactions in colloidal dispersions. The colloidal radial distribution functions for model colloid-polymer and colloid-colloid mixtures were measured with confocal microscopy. MC simulations that used established theoretical potentials, and included the measured polydispersity and intrinsic particle tracking error effects, quantitatively reproduce the experimental $g(r)$'s. We also inverted the radial distribution functions to extract effective potentials $u(r)$. For the colloid-polymer system, quantitative accuracy was affected by the polydispersity and tracking errors, but for the colloid-colloid system, we obtained near quantitative agreement with effective potentials derived from DFT.³⁶ In particular, we obtained the first *quantitative* agreement between measurements and the oscillations of the effective potential induced by 3D hard spheres. We also demonstrated the accuracy of the experimental technique by measuring, for the first time, the cross correlations $g_{\text{LS}}(r)$ between the large and the small colloids as well as $g_{\text{SS}}(r)$ the small-small radial distribution function. This may lead to the possibility of extracting effective potentials between particles of different sizes in a more complex mixture as well.

We believe our results demonstrate that our method may be used for measuring interactions in rather more general systems than the colloid-polymer mixture and binary “hard spheres” presented here. These trial model systems nevertheless prove a valuable test bed, since both are well described by theory. The quantitative agreement found in both cases underlines our confidence in this method.

That we find reasonable agreement in the case of a dynamically arrested state underlines observations that arrest is not always accompanied by a significant change in structure.⁴⁸ It is possible that dynamical arrest may be attrib-

uted to electrostatic interactions, whose effects on the structure are too subtle to cause significant changes to the radial distribution function. However, we note that the confocal image in Fig. 2(d) suggests medium-ranged order of the smaller particles, reminiscent of that seen in experiments⁴⁸ and simulations.^{49,50}

It is appropriate to consider the limitations of our approach. We have predominantly measured the so-called “energetic fluid regime,”²⁶ where $g(r) \approx \exp(-\beta u(r))$ provides a good approximation to the radial distribution function. This exponential sensitivity allows for accurate measurements of the potentials and for a simplified inversion procedure. We have worked at around 10% of the freezing volume fraction, in the case of hard spheres, and found very good agreement. Similar conclusions may be drawn from earlier work, where good agreement was found between Eq. (1) and experiment in the case of charged colloids, albeit at a correspondingly lower volume fraction.²⁸ At higher volume fractions, $g(r)$ becomes dominated by higher-order maxima which result from packing. Accurate reverse MC and integral equation techniques exist for inverting $g(r)$ outside of the energetic fluid regime. Exactly when these more sophisticated methods need to be used will depend on details of the system. Moreover, there are added subtleties to take into account. For some systems many-body potential effects can become increasingly pronounced for increasing densities.³¹ In addition, colloidal systems are always polydisperse, and inversion techniques for polydisperse fluids are not yet well established. Our results suggest that polydispersity will mask some “high frequency” features of the potentials.

We have measured relatively large colloids in a system optimized for confocal microscopy. Clearly, relatively greater inaccuracies in the particle tracking, for example, with smaller or nonrefractive index matched particles, will result in a less precise measure of the effective pair interaction. Moreover, it should be emphasized that the relevant length scale is the interaction range, set, for example, by the depletant size or Debye length rather than the actual colloid diameter itself. An advantage of our system over single particle techniques is that, because a larger number of colloids are being measured simultaneously, statistical averaging is more easily performed.

Finally, we believe that it is even possible to extend this technique beyond the spherically symmetric interactions we have considered so far to the newly emerging field of colloidal molecules^{51,52} and measure orientationally dependent distribution functions $g(r, \theta, \phi)$.

ACKNOWLEDGMENTS

The authors are grateful to Alfons van Blaaderen and Didi Derks for particle synthesis help and gifts. This work was partially supported by a grant-in-aid from the Ministry of Education, Culture, Sports, Science and Technology, Japan.

- ¹C. Likos, Phys. Rep. **348**, 267 (2001).
- ²J.-P. Hansen and I. Macdonald, *Theory of Simple Liquids* (Academic, London, 1976).
- ³D. Frenkel and B. Smit, *Understanding Molecular Simulation: From Algorithms to Applications* (Academic, New York, 2001).
- ⁴P. Pusey and W. van Meegen, Nature (London) **320**, 340 (1986).
- ⁵D. Frenkel, Science **296**, 65 (2002).
- ⁶W. C. K. Poon, J. Phys.: Condens. Matter **14**, R859 (2002).
- ⁷J. Joannopoulos, P. Villeneuve, and S. Fan, Nature (London) **386**, 143 (1997).
- ⁸V. Trappe, V. Prasad, P. Cipelletti, L. Segre, and D. Weitz, Nature (London) **411**, 772 (2001).
- ⁹J. P. K. Doye, A. A. Louis, I.-C. Lin, L. R. Allen, E. G. Noya, A. W. Wilber, H. C. Kok, and R. Lyus, Phys. Chem. Chem. Phys. **9**, 2197 (2007).
- ¹⁰G. Benedek, J. Pande, G. Thurston, and J. Clark, Prog. Retin Eye Res. **18**, 391 (1999).
- ¹¹J. Overbeek and E. Verwey, *Theory of the Stability of Lyophobic Colloids* (Elsevier, Amsterdam, 1949).
- ¹²S. Asakura and F. Oosawa, J. Chem. Phys. **22**, 1255 (1955).
- ¹³A. Vrij, Pure Appl. Chem. **48**, 471 (1976).
- ¹⁴Y. Monovoukis and A. Gast, J. Colloid Interface Sci. **128**, 533 (1989).
- ¹⁵C. Bechinger, D. Rudhardt, P. R. R. Leiderer, and S. Dietrich, Phys. Rev. Lett. **83**, 3960 (1999).
- ¹⁶M. Piech and J. Walz, J. Colloid Interface Sci. **253**, 117 (2002).
- ¹⁷J. Crocker and D. Grier, Phys. Rev. Lett. **81**, 352 (1994).
- ¹⁸R. Verma, J. Crocker, T. Lubensky, and A. Yodh, Phys. Rev. Lett. **81**, 4004 (1998).
- ¹⁹J. Crocker, J. Matteo, A. Dinsmore, and A. Yodh, Phys. Rev. Lett. **83**, 4352 (1999).
- ²⁰J. Baumgartl and C. Bechinger, Europhys. Lett. **71**, 487 (2005).
- ²¹A. Ramirez-Saito, C. Bechinger, and J. Arauz-Lara, Phys. Rev. E **74**, 030401 (2006).
- ²²D. Vossen, Ph.D. thesis, Utrecht University, 2004 (URL Phdthesis, www.colloid.nl/Theses/ThesisVossen2004.pdf).
- ²³M. H. G. Duits, R. P. May, A. Vrij, and C. G. De Kruif, Langmuir **7**, 62 (1991).
- ²⁴X. Ye, T. Narayanan, P. Tong, and J. S. Huang, Phys. Rev. Lett. **76**, 4640 (1996).
- ²⁵R. Baxter, J. Chem. Phys. **49**, 2770 (1968).
- ²⁶A. Louis, Philos. Trans. R. Soc. London, Ser. A **359**, 939 (2001).
- ²⁷A. van Blaaderen and P. Wiltzius, Science **270**, 1177 (1995).
- ²⁸C. P. Royall, M. E. Leunissen, and A. van Blaaderen, J. Phys.: Condens. Matter **15**, S3581 (2003).
- ²⁹J. Baumgartl, R. P. A. Dullens, M. Dijkstra, R. Roth, and C. Bechinger, Phys. Rev. Lett. **98**, 198303 (2007).
- ³⁰M. Brunner, C. Bechinger, W. Strepp, V. Lobaskin, and H. H. von Gruenberg, Europhys. Lett. **58**, 926 (2002).
- ³¹A. Louis, J. Phys.: Condens. Matter **14**, 9187 (2002).
- ³²C. Russ, M. Brunner, C. Bechinger, and H. H. von Gruenberg, Europhys. Lett. **69**, 468 (2005).
- ³³K. Zahn, G. Maret, C. Russ, and H. H. von Gruenberg, Phys. Rev. Lett. **91**, 115502 (2003).
- ³⁴N. G. Almarza and E. Lomba, Phys. Rev. E **68**, 011202 (2003).
- ³⁵A. Louis, e-print arXiv:cond-mat/0212073.
- ³⁶R. Roth, R. Evans, and S. Dietrich, Phys. Rev. E **62**, 5360 (2000).
- ³⁷G. Bosma, C. Pathmamanoharan, E. H. A. de Hoog, W. K. Kegel, A. van Blaaderen, and H. N. W. Lekkerkerker, J. Colloid Interface Sci. **245**, 292 (2002).
- ³⁸B. Vincent, Colloids Surf. **50**, 241 (1990).
- ³⁹G. Berry, J. Chem. Phys. **44**, 4550 (1966).
- ⁴⁰C. Royall, D. Aarts, and H. Tanaka, J. Phys.: Condens. Matter **17**, S3401 (2005).
- ⁴¹P. J. Lu, J. C. Conrad, H. M. Wyss, A. B. Schofield, and D. A. Weitz, Phys. Rev. Lett. **96**, 028306 (2006).
- ⁴²A. Louis, P. Bolhuis, E. Meijer, and J.-P. Hansen, J. Chem. Phys. **117**, 1893 (2002).
- ⁴³B. Widom, J. Chem. Phys. **39**, 2808 (1963).
- ⁴⁴A. Yethiraj and A. van Blaaderen, Nature (London) **421**, 513 (2003).
- ⁴⁵C. Royall, M. Leunissen, A.-P. Hynninen, M. Dijkstra, and A. van Blaaderen, J. Chem. Phys. **124**, 244706 (2006).

⁴⁶D. Goulding and J.-P. Hansen, *Mol. Phys.* **99**, 865 (2001).

⁴⁷J. Mendel, *Maximum-likelihood Deconvolution: A Journey into Model-Based Signal Processing* (Springer-Verlag, New York, 1990).

⁴⁸N. Simeonova, R. Dullens, D. Aarts, H. de Villeneuve, V. W. A. Lekkerkerker, and W. Kegel, *Phys. Rev. E* **73**, 041401 (2006).

⁴⁹H. Shintani and H. Tanaka, *Nat. Phys.* **2**, 200 (2006).

⁵⁰T. Hamanaka and A. Onuki, *Phys. Rev. E* **75**, 041503 (2007).

⁵¹V. N. Manoharan, M. T. Elessar, and D. J. Pine, *Science* **301**, 483 (2003).

⁵²P. Johnson, C. van Katz, and A. van Blaaderen, *Langmuir* **21**, 11510 (2005).